Curvature delays growth-induced wrinkling

Document Version
Accepted author manuscript

[Link to publication record in Manchester Research Explorer](#)

Citation for published version (APA):
Jia, F., Pearce, S., & Goriely, A. (2018). Curvature delays growth-induced wrinkling. *Physical Review E - Statistical, Nonlinear, and Soft Matter Physics*, *98*(3), [033003]. https://doi.org/10.1103/PhysRevE.98.033003

Published in:
Physical Review E - Statistical, Nonlinear, and Soft Matter Physics

OPEN ACCESS

Curvature delays growth-induced wrinkling

Fei Jia[1,3], Simon P. Pearce[2], Alain Goriely[3]

[1]*School of Manufacturing Science and Engineering,
Southwest University of Science and Technology,
Sichuan 621010, China;*
[2]*School of Mathematics and the Faculty of Biology,
Medicine and Health,
The University of Manchester,
Manchester M13 9PL, UK;*
[3]*Mathematical Institute, University of Oxford,
Oxford OX2 6GG, UK.*
(Dated: October 5, 2018)

Wrinkling patterns can be induced by the growth of a thin elastic film over a soft elastic substrate. While there is a good understanding of how this pattern is initiated on a flat geometry, wrinkling patterns over a curved surface are more complicated. Here, we consider this phenomenon within the framework of large deformation morphoelasticity by investigating surface wrinkling of a growing thin elastic film bonded to a large elastic cylinder. The system has two important dimensionless parameters: the ratio η of the film thickness by the cylinder radius and the relative stiffness of the two layers ξ. Depending on the values of ξ and η we identify four different regimes for which we find the critical growth and wrinkling mode number. By combining asymptotic methods with numerical computations we determine the effect of the curvature on the bifurcation and establish that it always induces a delay at the bifurcation: larger growth is needed on a curved surface to induce the same wrinkling instability. These results are crucial to understand pattern formation on surface with varying curvatures.

INTRODUCTION

Surface morphological instabilities of soft materials caused by growing or swelling have been a subject of considerable interest over the last few years as this has been proposed as a key mechanism for morphogenesis and for the control of engineered thin-film materials [1–10]. Typically, these instabilities are driven by differential expansion of two bonded layers. In this case a stability analysis can be used to determine the critical conditions for the onset of surface wrinkling. These ideas have been applied to different geometries such as planar films [11–14], cylindrical shells [15–17], and spherical layers [18–21]. Comparisons between planar and curved systems reveal that the surface curvature plays an important role in pattern formation and evolution. Most of these previous studies either focused on the various wrinkling modes on a curved surface [13, 18, 20], or emphasise the use of effective numerical methods for complex geometries [19, 22].

A key question is to understand the relative effect of curvature on the wrinkling bifurcation. There have been various studies on reduced systems such as growing rods [8] in which a modified beam equation was derived to take the curvature of the substrate into account. For elastic shells, Cai et al. [13] adopted the Donnell-Mushtari-Vlassov shell equation to explain the occurrence of hexagonal modes on a slightly curved surface. They showed that both the critical stress and wave-number are related to a curvature parameter Ω to order Ω^2 when $\Omega \ll 1$.

Yet, the problem has not been fully investigated within the framework of nonlinear elasticity where precise state-ments can be obtained. To address this question, we study the problem of the circumferential wrinkling of a growing thin cylindrical shell on a softer non-growing cylinder. We assume that both materials are isotropic, incompressible and hyperelastic and look for plane-strain solutions that are essentially two dimensional (since it is assumed that there is no deformation in the third dimension). We are particularly interested in the comparison between the cylindrical and planar cases that can be obtained as the limit when the ratio between film thickness and the cylinder radius goes to 0. Here, we clarify the role of curvature on the critical growth and mode number. There are two important dimensionless parameters in the system: the ratio of the film thickness h to the cylinder radius R and the ratio of elastic shear modulus of the film μ_{f}, to the shear modulus of the substrate μ_{s}:

$$\eta = \frac{h}{R}, \quad \text{and} \quad \xi = \frac{\mu_{\mathrm{f}}}{\mu_{\mathrm{s}}}. \tag{1}$$

Since we are interested in thin films, we assume $\eta \ll 1$. There are then four regimes of interest: either $\xi = O(1)$, $\xi = O(\eta^{-1})$, $\xi = O(\eta^{-3})$, or $\xi \gg O(\eta^{-3})$. The case for which $\xi = O(\eta^{-1})$ has already been studied in [13, 23]. To the best of our knowledge, the case where stiffnesses are comparable $\xi = O(1)$ with $\eta \ll 1$ has not been discussed. In this case, the circumferential wrinkling mode number is large which causes numerical difficulties. However, the Wentzel-Kramers-Brillouin (WKB) method [24, 25] can be used to obtain excellent approximations to the solutions. In the remaining two cases, $\xi = O(\eta^{-3})$, or $\xi \gg O(\eta^{-3})$, the wrinkling mode number is relatively
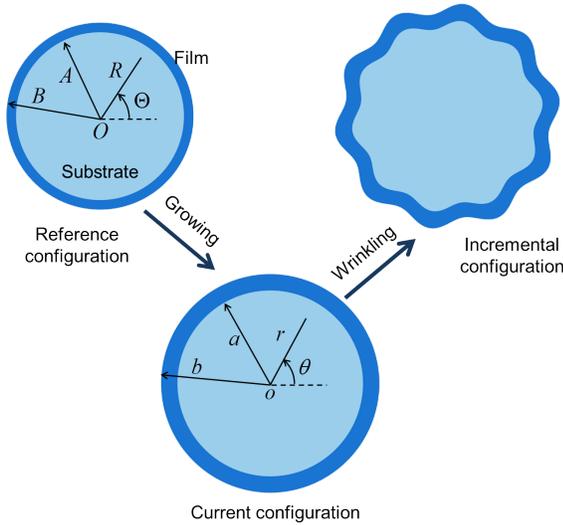
FIG. 1. Cylindrical film-substrate model. In plane strain, there is no deformation along the axis and a material point position is specified by its position in the reference (R, Θ) and current (r, θ) configurations.

small and a regular perturbation analysis is used to obtain estimates on the critical growth and mode number. Taken together, the results of these analyses give a complete picture of the role of curvature in the wrinkling instability of thin films on a curved substrate valid for all stiffness ratios. Finally, we note that there is a well-know limit in the planar case. If the film is sufficiently soft then the first instability that takes place is the so-called *Biot instability* [31] with a mode with vanishing wavelength. Therefore, we expect that on a curved substrate, for sufficiently soft film, the Biot instability will also appear. This provides an upper bound for the stiffness ratio after which no wrinkling instability with finite wavelength is expected.

THEORETICAL SET-UP

Geometry

A cylinder is separated into two parts: a soft solid substrate and a hard film, as shown in Fig. 1. We assume that there is no deformation along the direction of the cylinder axis, so that the problem reduces to a plane-strain problem. The polar coordinates of a material point are $\{R, \Theta\}$ in the reference configuration and $\{r, \theta\}$ in the current configuration. The outer radii of the substrate and film before deformation are A, B, respectively. After deformation, the same radii are a and b, respectively.

Kinematics of deformation

We use the theory of morphoelasticity [3, 26] to describe deformations of a body that can both grow and deform elastically. We consider deformations $\boldsymbol{\chi} : \mathcal{B}_0 \to \mathcal{B}$ of a system in an initial configuration $\mathcal{B}_0$ to the current configuration $\mathcal{B}$. The deformation gradient is given by

$$\mathbf{F} = \mathrm{Grad}\boldsymbol{\chi}, \tag{2}$$

where the gradient is taken with respect to coordinates in the reference configuration. The fundamental assumption of morphoelasticity is that this deformation gradient can be multiplicatively decomposed into a growth deformation tensor $\mathbf{G}$ and an elastic deformation tensor $\mathbf{A}$:

$$\mathbf{F} = \mathbf{A}\mathbf{G}. \tag{3}$$

For the particular geometry under consideration, we assume that the growth tensors $\mathbf{G}$ in both substrate and film have the form:

$$\mathbf{G}_{\mathrm{s}} = \begin{bmatrix} g_{1\mathrm{s}} & 0 \\ 0 & g_{2\mathrm{s}} \end{bmatrix}, \qquad \mathbf{G}_{\mathrm{f}} = \begin{bmatrix} g_{1\mathrm{f}} & 0 \\ 0 & g_{2\mathrm{f}} \end{bmatrix}. \tag{4}$$

Here and in the remainder of this paper, the subscripts 's' and 'f' are used to describe variables attached to the substrate and film, respectively.

Energy functions and stress tensors

Both materials are assumed to be incompressible, hyperelastic and isotropic. Since only the elastic part of the deformation stores elastic energy, we assume that the strain-energy density function of the material depends on $\mathbf{A}$ only. In our study, we choose a Neo-Hookean material

$$W_{\mathrm{s}} = \frac{\mu_{\mathrm{s}}}{2}(I_1 - 2), \qquad W_{\mathrm{f}} = \frac{\mu_{\mathrm{f}}}{2}(I_1 - 2). \tag{5}$$

Here $I_1 = \mathrm{Tr}(\mathbf{C})$, where $\mathbf{C} = \mathbf{A}^{\mathsf{T}}\mathbf{A}$ is the principal invariant associated with the right Cauchy-Green tensor $\mathbf{C}$.

Once the strain-energy density function is defined, the stress tensors can be obtained. The nominal stress tensor $\mathbf{S}$ is [3]

$$\mathbf{S} = J\mathbf{G}^{-1}\frac{\partial W}{\partial \mathbf{A}} - pJ\mathbf{G}^{-1}\mathbf{A}^{-1}, \tag{6}$$

where the local volume increase $J = \det \mathbf{F} = \det \mathbf{G}$, and p is the Lagrange multiplier associated with incompressibility and can be identified with the hydrostatic pressure. In components, we have

$$\begin{aligned}
\left(\frac{\partial W(\mathbf{C})}{\partial \mathbf{A}}\right)_{ij} &= \frac{\partial W(\mathrm{A}_{lk}\mathrm{A}_{lm})}{\partial \mathrm{A}_{ji}} \\
&= \frac{\partial W(\mathbf{C})}{\partial \mathrm{C}_{km}}\frac{\partial \mathrm{A}_{lk}\mathrm{A}_{lm}}{\partial \mathrm{A}_{ji}} = \frac{\partial W(\mathbf{C})}{\partial \mathrm{C}_{im}}\mathrm{A}_{jm} + \frac{\partial W(\mathbf{C})}{\partial \mathrm{C}_{ki}}\mathrm{A}_{jk} \\
&= \left(\frac{\partial W(\mathbf{C})}{\partial \mathbf{C}}\right)_{mi}\mathrm{A}_{jm} + \left(\frac{\partial W(\mathbf{C})}{\partial \mathbf{C}}\right)_{ik}\mathrm{A}_{jk}.
\end{aligned} \tag{7}$$

Then

$$\frac{\partial W}{\partial \mathbf{A}} = \left(\left(\frac{\partial W}{\partial \mathbf{C}} \right)^{\mathsf{T}} + \frac{\partial W}{\partial \mathbf{C}} \right) \mathbf{A}^{\mathsf{T}}, \qquad (8)$$

and as $\mathbf{C}$ is a symmetric tensor, $\partial W / \partial \mathbf{C}$ is also a symmetric tensor with

$$\frac{\partial W}{\partial \mathbf{A}} = 2 \frac{\partial W}{\partial \mathbf{C}} \mathbf{A}^{\mathsf{T}}. \qquad (9)$$

So the nominal stress (6) can be written

$$\mathbf{S} = 2J\mathbf{G}^{-1} \frac{\partial W}{\partial \mathbf{C}} \mathbf{A}^{\mathsf{T}} - pJ\mathbf{G}^{-1}\mathbf{A}^{-1}. \qquad (10)$$

For the strain-energy density function (5), the stress is

$$\mathbf{S} = \mu J \mathbf{G}^{-1} \mathbf{A}^{\mathsf{T}} - pJ\mathbf{G}^{-1}\mathbf{A}^{-1}, \qquad (11)$$

From the nominal stress tensor, we obtain the Cauchy stress tensor as follows:

$$\mathbf{T} = J^{-1} \mathbf{F} \mathbf{S} = \mu \mathbf{A} \mathbf{A}^{\mathsf{T}} - p\mathbf{I}, \qquad (12)$$

The equilibrium equation can be written either in terms of $\mathbf{S}$ or $\mathbf{T}$ as

$$\text{Div}\,\mathbf{S} = \mathbf{0} \quad \text{or} \quad \text{div}\,\mathbf{T} = \mathbf{0}, \qquad (13)$$

where the divergence Div (resp. div) is taken in the reference (resp. current) configuration.

Equilibrium state

For an axisymmetric deformation of the form

$$r = r(R), \quad \Theta = \theta, \qquad (14)$$

the deformation gradient reads [3, p. 273]

$$\mathbf{F} = \begin{bmatrix} r_{,R} & 0 \\ 0 & r/R \end{bmatrix}, \qquad (15)$$

where the comma denotes partial differentiation: $r_{,R} \equiv \partial r / \partial R$. From the multiplicative decomposition, we obtain

$$\mathbf{A} = \begin{bmatrix} r_{,R}/g_1 & 0 \\ 0 & r/(g_2 R) \end{bmatrix} = \begin{bmatrix} \alpha_1 & 0 \\ 0 & \alpha_2 \end{bmatrix}. \qquad (16)$$

The incompressibility condition imposes

$$\det(\mathbf{A}) = 1 \Rightarrow r_{,R} \frac{r}{R} = g_1 g_2 = J. \qquad (17)$$

Solving (17), with the boundary condition $R = 0$, $r_\mathrm{s} = 0$, we obtain:

$$\begin{cases} r_\mathrm{s}^2 = J_\mathrm{s} R^2 & 0 \leq R < A, \\ r_\mathrm{f}^2 = J_\mathrm{f} R^2 + c_{1\mathrm{f}} & A \leq R \leq B. \end{cases} \qquad (18)$$

The continuity of displacement at the interface $R = A$ implies

$$J_\mathrm{s} A^2 = J_\mathrm{f} A^2 + c_{1\mathrm{f}} \Rightarrow c_{1\mathrm{f}} = (J_\mathrm{s} - J_\mathrm{f}) A^2, \qquad (19)$$

and

$$\begin{aligned} \alpha_\mathrm{s} &= \frac{r_\mathrm{s}}{g_{2\mathrm{s}} R} = \frac{r_\mathrm{s}}{\sqrt{\lambda_\mathrm{s}} r_\mathrm{s}} = \frac{1}{\sqrt{\lambda_\mathrm{s}}}, \\ \alpha_\mathrm{f} &= \frac{r_\mathrm{f}}{g_{2\mathrm{f}} R} = \frac{r_\mathrm{f}}{\sqrt{\lambda_\mathrm{f}(r_\mathrm{f}^2 - c_{1\mathrm{f}})}}, \end{aligned} \qquad (20)$$

where $\lambda = g_2 / g_1$.

We note that from (20) we have $\alpha_{\mathrm{s},r} = 0$. This last identity can be written formally as $\alpha_{\mathrm{s},r} = (1 - \lambda_\mathrm{s} \alpha_\mathrm{s}^2) \alpha_\mathrm{s}/r$. Therefore, we have

$$\alpha_{\mathrm{s},r} = \frac{\alpha_\mathrm{s}(1 - \lambda_\mathrm{s} \alpha_\mathrm{s}^2)}{r}, \qquad (21)$$

$$\alpha_{\mathrm{f},r} = \frac{\alpha_\mathrm{f}(1 - \lambda_\mathrm{f} \alpha_\mathrm{f}^2)}{r}, \qquad (22)$$

which can be written in general, as

$$\alpha_{,r} = \frac{\alpha(1 - \lambda \alpha^2)}{r}. \qquad (23)$$

We can now solve the equilibrium equation. The Cauchy stress tensor for this axisymmetric deformation is also diagonal with $\mathbf{T} = \text{diag}(\mathrm{T}_{rr}, \mathrm{T}_{\theta\theta})$ and (13) reduces to a single non-trivial equation

$$\frac{\partial \mathrm{T}_{rr}}{\partial r} + \frac{\mathrm{T}_{rr} - \mathrm{T}_{\theta\theta}}{r} = 0. \qquad (24)$$

Using the particular form (12), we solve (24) to obtain

$$p_{,r} = \mu \frac{\partial \alpha^{-2}}{\partial r} + \frac{\mu(\alpha^{-2} - \alpha^2)}{r}. \qquad (25)$$

Equation (25) can be integrated once to give $p(r) = f(r) + c_2$, where

$$f(r) = \begin{cases} \mu_\mathrm{s} \left(\alpha_\mathrm{s}^{-2} + \frac{\lambda_\mathrm{s}^2 - 1}{\lambda_\mathrm{s}} \ln r \right), \\ \mu_\mathrm{f} \left[\alpha_\mathrm{f}^{-2} - \frac{\lambda_\mathrm{f} c_{1\mathrm{f}}}{2r^2} + \lambda_\mathrm{f} \ln r - \frac{\ln(c_{1\mathrm{f}} + r^2)}{2\lambda_\mathrm{f}} \right], \end{cases} \qquad (26)$$

and the constants $c_{2\mathrm{f}}$, $c_{2\mathrm{s}}$ are to be determined from the boundary conditions.

Stability analysis

We consider incremental perturbations around a stationary homogeneous state changing the displacement from the homogeneous solution $\boldsymbol{\chi}$ to the perturbed displacement $\boldsymbol{\chi} + \delta\mathbf{x}$. The corresponding deformation gradient changes from $\mathbf{F}$ to $\mathbf{F} + \delta\mathbf{F}$. To this incremental deformation gradient, we associate an elastic deformation tensor $\delta\mathbf{A} = (\delta\mathbf{F})\mathbf{G}^{-1}$. This incremental deformation

gradient contains information about the perturbed non-homogeneous solution. In the following, it is advantageous to reformulate this tensor in the current configuration by its pull-forward: $\delta\mathbf{F} = (\delta\mathbf{F}_c)\mathbf{F}$ and $\delta\mathbf{A} = (\delta\mathbf{F}_c)\mathbf{A}$. The incremental form (13) of the equilibrium equations [26, 27] can be written in terms of the nominal stress tensor $\mathbf{S}$ as

$$\text{Div}\,\delta\mathbf{S} = \mathbf{0}, \tag{27}$$

From (10),

$$\delta\mathbf{S} = J\mathbf{G}^{-1}\left[2\delta\left(\frac{\partial W}{\partial\mathbf{C}}\mathbf{A}^{\mathsf{T}}\right) - \delta\left(p\mathbf{A}^{-1}\right)\right]$$
$$= J\mathbf{G}^{-1}\left[2\delta\left(\frac{\partial W}{\partial\mathbf{C}}\right)\mathbf{A}^{\mathsf{T}} + 2\frac{\partial W}{\partial\mathbf{C}}\delta\mathbf{A}^{\mathsf{T}}\right.$$
$$\left. - \delta p\mathbf{A}^{-1} - p\delta\mathbf{A}^{-1}\right]. \tag{28}$$

The tensor $\delta(\partial W/\partial\mathbf{C})$ can be written in component form as,

$$\delta\left(\frac{\partial W}{\partial\mathbf{C}}\right)_{ijkl} = \frac{\partial^2 W}{\partial\mathrm{C}_{ji}\partial\mathrm{C}_{lk}}\delta\mathrm{C}_{lk} = \frac{\partial^2 W}{\partial\mathrm{C}_{ji}\partial\mathrm{C}_{lk}}\delta\mathrm{C}_{kl}, \tag{29}$$

and hence

$$\delta\left(\frac{\partial W}{\partial\mathbf{C}}\right) = \frac{\partial^2 W}{\partial\mathbf{C}\partial\mathbf{C}} : \delta\mathbf{C}. \tag{30}$$

Using $\delta(\mathbf{A}\mathbf{A}^{-1}) = \mathbf{0}$, we therefore have

$$\delta\left(\mathbf{A}^{-1}\right) = -\mathbf{A}^{-1}\delta\mathbf{A}\mathbf{A}^{-1} \tag{31}$$

Substituting (30) and (31) into (28), the incremental form of $\mathbf{S}$ is

$$\delta\mathbf{S} = J\mathbf{G}^{-1}\left[2\left(\frac{\partial^2 W}{\partial\mathbf{C}\partial\mathbf{C}} : \delta\mathbf{C}\right)\mathbf{A}^{\mathsf{T}}\right.$$
$$\left. + 2\frac{\partial W}{\partial\mathbf{C}}\mathbf{A}^{\mathsf{T}}\delta\mathbf{F}_c^{\mathsf{T}} - \delta p\mathbf{A}^{-1} + p\mathbf{A}^{-1}\delta\mathbf{F}_c\right], \tag{32}$$

where $\delta\mathbf{C} = (\delta\mathbf{A})^{\mathsf{T}}\mathbf{A} + \mathbf{A}^{\mathsf{T}}\delta\mathbf{A}$. In the current configuration, (27) becomes

$$\text{div}\,\delta\mathbf{S}_0 = \mathbf{0}, \tag{33}$$

where

$$\delta\mathbf{S}_0 = J^{-1}\mathbf{F}\delta\mathbf{S} \tag{34}$$

For the strain-energy density function (5), the first term in $\delta\mathbf{S}_0$ vanishes identically, so that

$$\delta\mathbf{S}_0 = \mu\mathbf{A}\mathbf{A}^{\mathsf{T}}(\delta\mathbf{F}_c)^{\mathsf{T}} - \delta p\,\mathbf{I} + p\,\delta\mathbf{F}_c. \tag{35}$$

The boundary and continuity conditions are

$$\delta\mathbf{S}_0^{\mathsf{T}}\mathbf{n} = \mathbf{0} \qquad \text{at } r = b, \tag{36}$$
$$[[\delta\mathbf{x}]] = \mathbf{0} \text{ and } [[\delta\mathbf{S}_0^{\mathsf{T}}\mathbf{n}]] = \mathbf{0} \quad \text{at } r = a, \tag{37}$$
$$\delta\mathbf{x} = \mathbf{0} \text{ at } r = 0, \tag{38}$$

where $[[\cdot]]$ represents a jump of the argument across the interface,

$$[[\cdot]] = \lim_{\substack{R\to A \\ R>A}}(\cdot) - \lim_{\substack{R\to A \\ R<A}}(\cdot). \tag{39}$$

The incremental displacement can be written:

$$\delta\mathbf{x} = u(r,\theta)\mathbf{e}_r + v(r,\theta)\mathbf{e}_\theta. \tag{40}$$

where, for a single mode,

$$u(r,\theta) = U(r)\cos(n\theta), \qquad v(r,\theta) = V(r)\sin(n\theta). \tag{41}$$

Similarly, the incremental form of the pressure δp is

$$\delta p(r,\theta) = P(r)\cos(n\theta). \tag{42}$$

In components $\delta\mathbf{F}_c$ reads

$$\delta\mathbf{F}_c = \begin{bmatrix} u_{,r} & \frac{u_{,\theta}-v}{r} \\ v_{,r} & \frac{v_{,\theta}+u}{r} \end{bmatrix}. \tag{43}$$

The incompressibility constraint implies $\text{tr}(\delta\mathbf{F}_c) = 0$:

$$u_{,r} + \frac{v_{,\theta}+u}{r} = 0. \tag{44}$$

After simplification the equation for $U = U(r)$ is

$$U'''' + M_3 U''' + M_2 U'' + M_1 U' + M_0 U = 0 \tag{45}$$

where

$$M_0 = \frac{(n^2-1)(3 - 4\lambda\alpha^2 + n^2\alpha^4)}{r^4},$$
$$M_1 = \frac{3 + n^2 - 2\lambda(n^2+2)\alpha^2 - 3n^2\alpha^4 + 2\lambda n^2\alpha^6}{r^3},$$
$$M_2 = -\frac{3 + n^2 - 8\lambda\alpha^2 + n^2\alpha^4}{r^2}, \quad M_3 = \frac{2 + 4\lambda\alpha^2}{r}.$$

The boundary conditions, written in terms of $U(r)$, are

- At $r = b$, the incremental stresses on the film surface vanish:

$$U''' + M_4 U'' + M_5 U' + M_6 U = 0,$$
$$U'' + \frac{1}{r}U' + \frac{(n^2-1)}{r^2}U = 0. \tag{46}$$

  where

$$M_4 = \frac{2 + 2\lambda\alpha^2}{r},$$
$$M_5 = -\frac{1 + 2n^2 - 2\lambda\alpha^2 + n^2\alpha^4}{r^2},$$
$$M_6 = \frac{(n^2-1)(2\lambda\alpha^2 - 1)}{r^3}.$$

All the parameters in the last two equations are for the film.

- At the interface $r = a$, the incremental displacements and stresses satisfy the continuity condition: $[[U]] = 0$, $[[U']] = 0$. Further, we have $(\delta\mathbf{S}_{0f})_{11} = (\delta\mathbf{S}_{0s})_{11}$, $(\delta\mathbf{S}_{0f})_{21} = (\delta\mathbf{S}_{0s})_{21}$ so that

$$\left[\left[\frac{\mu}{\alpha^2}\left(U''' + M_4 U'' + M_5 U' + M_6 U = 0\right)\right]\right] = 0,$$
$$\left[\left[\frac{\mu}{\alpha^2}\left(U'' + \frac{1}{r}U' + \frac{(n^2-1)}{r^2}U\right)\right]\right] = 0. \tag{47}$$

- At the center $r = 0$, we have $U = 0$, $U' = 0$.

The problem studied in this paper is to obtain information on the solutions of the system (45) of two fourth-order ODEs (one for the film and one for the substrate) coupled by the above boundary conditions. We restrict our attention to isotropic growth in the film and no growth in the substrate. Thus $g_{1f} = g_{2f} =: g$, $g_{1s} = g_{2s} = 1$ and $\lambda_f = \lambda_s = 1$.

Without loss of generality, we set the radius of the substrate to $A = 1$, and scale all the stress components by μ_s. We introduce two dimensionless numbers : the stiffness ratio $\xi = \mu_f/\mu_s$ and the aspect ratio between the film thickness and the cylinder radius $\eta = (B-A)/A = B-1$. Since we assume that the film is thin, we have $\eta \ll 1$. In the following, we identify four regimes of interest, depending on the relative size of ξ with respect to η.

LARGE MODE NUMBERS: WKB METHOD

First, we look for a solution of (45) by using the WKB method following [23]. This approach is valid for large values of n. The general ansatz for U_f of the film is then

$$U_f = \sum_{i=1}^{4} K_i \exp\left(\int_r^b S_f^{(i)}(r)\mathrm{d}r\right),$$
$$S_f^{(i)} = n S_{f0}^{(i)} + S_{f1}^{(i)} + O(n^{-1}), \quad (a \le r \le b), \tag{48}$$

where after substitution in (45), we find

$$S_{f0}^{(1)} = \frac{1}{r}, \ \ S_{f0}^{(2)} = -\frac{1}{r}, \ \ S_{f0}^{(3)} = \frac{\alpha_f^2}{r}, \ \ S_{f0}^{(4)} = -\frac{\alpha_f^2}{r},$$
$$S_{f1}^{(1)} = S_{f1}^{(2)} = -\frac{(\alpha_f^2-1)(\alpha_f^4+1)}{r(\alpha_f^4-1)},$$
$$S_{f1}^{(3)} = S_{f1}^{(4)} = -\frac{2\alpha_f^4(\alpha_f^2-1)}{r(\alpha_f^4-1)}, \cdots$$

and the constants K_i are to be determined from the boundary conditions.

For the substrate with $g_s = 1$, $\lambda_s = 1$ and $\alpha_s = 1$, (45) simplifies to

$$U_s'''' + \frac{6}{r}U_s''' - \frac{2n^2-5}{r^2}U_s'' - \frac{2n^2+1}{r^3}U_s'$$
$$+ \frac{(n^2-1)^2}{r^4}U_s = 0, \tag{49}$$

with general solution

$$U_s = K_5 U_s^{(1)} + K_6 U_s^{(2)} + K_7 U_s^{(3)} + K_8 U_s^{(4)}, \tag{50}$$

where

$$U_s^{(1)} = r^{n+1}, \qquad U_s^{(2)} = r^{n-1},$$
$$U_s^{(3)} = r^{-n-1}, \quad U_s^{(4)} = r^{-n+1}. \tag{51}$$

The boundary condition at $r = 0$ implies that $K_7 = K_8 = 0$. Thus, U_s can be written as

$$U_s = K_5 U_s^{(1)} + K_6 U_s^{(2)}. \tag{52}$$

On substituting (48–52) into the boundary conditions (46–47), we obtain six equations for the constants K_i that can be written in a compact form as

$$\mathbf{M}\,\mathbf{K} = \mathbf{0}, \qquad \mathbf{K} = (K_1, K_2, K_3, K_4, K_5, K_6)^{\mathsf{T}}, \tag{53}$$

where the matrix $\mathbf{M}$ is given in Appendix A. Finally the bifurcation condition is given by

$$\mathbf{f}(\xi, g, B, n) \equiv \det(\mathbf{M}) = 0. \tag{54}$$

And the equation setting the critical mode number n_c is given by

$$\mathbf{h}(\xi, g, B, n) \equiv \frac{\partial \mathbf{f}(\xi, g, B, n)}{\partial n} = 0. \tag{55}$$

A THIN FILM ON A LARGE CYLINDER

Here, we focus on the case $\eta = B - 1 \ll O(1)$, which corresponds to a film that is very thin compared to the radius of the cylinder. The limiting case $\eta \to 0$ is that of a film on a flat substrate. Our main focus is to investigate the effect of a small curvature on the instability of a film on a flat substrate. In particular, we are interested in the influence of the curvature on the critical growth g_c and critical mode number n_c. Note that the definition of n_c is different from the generally used wave number k_c, but they are related as follows: $n_c = k_c R_0$, where R_0 is the radius of the middle surface of the film in the reference configuration. Then, we have $k_c h = n_c h/R_0$. Under the assumption $\eta \ll O(1)$, R_0 should be approximately equal to the radius of the substrate $A = 1$. Thus, we have $k_c h \approx n_c h/A = n_c \eta$, which is a key parameter for characterizing the instability. Therefore, in our discussion, we will use $n_c \eta$ instead of n_c.

A moderately stiff film on a soft substrate
S2: $\xi = O(\eta^{-1})$

Rather than starting with the case S1, for completeness, we discuss briefly the case $\xi = O(\eta^{-1})$ that has

already been presented in [23]. There are four small parameters in the problem: $1/\xi, 1/n, \eta$ and $\epsilon = g-1$. Equations (54) and (55) can be doubly expanded in ϵ and η.

$$(12 + 48\eta + 24n^2\eta^2) + (24\eta n + 16\eta^3 n^3)\xi + (-12\eta^2$$
$$+4\eta^4 n^4)\xi^2 + \Big[(48 + 168\eta^2 n^2) + 144\eta n\xi + (-48\eta^2 n^2$$
$$-96\eta^3 n^2 + 32\eta^4 n^4)\xi^2\Big]\epsilon + \ldots = 0, \tag{56}$$

$$48\eta n + (24 + 48\eta^2 n^2)\xi + 16\eta^3 n^3\xi^2 + \Big[336\eta n + 144\xi$$
$$+(-96\eta n - 192\eta^2 n + 128\eta^3 n^3)\xi^2\Big]\epsilon + \ldots = 0. \tag{57}$$

Using the leading-order balance and principle of least degeneracy we can deduce the relative balance of ϵ and n with respect to ξ and η. The leading-order terms in (56) can come from five terms 12, $24\eta n\xi$, $-12\eta^2\xi^2$, $4\eta^4 n^4\xi^2$ and $-48\eta^2 n^2\xi^2\epsilon$ and the corresponding three leading-order terms for (57) can come from 24ξ, $16\eta^3 n^3\xi^2$ and $-96\eta n\xi^2\epsilon$. Balancing these last three terms leads to $\eta n = O(\xi^{-\frac{1}{3}})$ and $\epsilon = O(\xi^{-\frac{2}{3}})$. Under these order relations, the leading term in (56) is of $O(\xi^{\frac{2}{3}})$ and we conclude that $\epsilon = O(\xi^{-\frac{2}{3}})$, $\eta = O(\xi^{-1})$, $n = O(\xi^{\frac{2}{3}})$. Since $B = 1 + \eta$ we can write

$$B = 1 + \frac{b_0}{\xi}, \tag{58}$$

where b_0 is a constant of $O(1)$ and seek an asymptotic solution for g_c and n_c in the form

$$g_c = 1 + \xi^{-\frac{2}{3}}(x_0 + x_1\xi^{-\frac{1}{3}} + x_2\xi^{-\frac{2}{3}} + \cdots),$$
$$n_c = \xi^{\frac{2}{3}}(y_0 + y_1\xi^{-\frac{1}{3}} + y_2\xi^{-\frac{2}{3}} + \cdots), \tag{59}$$

where the coefficients x_i and y_i $(i = 0, 1, 2, \cdots)$ can be deduced from (54) and (55). After simplification, we obtain

$$g_c = 1 + \frac{3^{2/3}}{4\xi^{2/3}} + \frac{17 \times 3^{1/3}}{160\xi^{4/3}} - \frac{3^{1/3}\xi^{2/3}}{12}\eta^2$$
$$-\frac{3^{2/3}}{4\xi^{2/3}}\eta + O(\eta^2), \tag{60}$$

$$n_c = \frac{3^{1/3}}{\xi^{1/3}\eta} - \frac{\xi}{3}\eta - \frac{11}{10\xi\eta} + \frac{3^{1/3}}{2\xi^{1/3}} + O(\eta^{2/3}).$$

A soft film on a soft substrate S1: $\xi = O(1)$

For a soft film on a soft substrate, the leading order terms in (57) can come from $48\eta n$, 24ξ, $16\eta^3 n^3\xi^2$ and $-96\eta n\xi^2\epsilon$. Clearly, the first term $48\eta n$ has higher order than the last term $-96\eta n\xi^2\epsilon$, except when $\epsilon = O(1)$. This implies that g_c cannot be chosen to be around 1, and we denote this as g_0 and obtain it later. From the first three terms, we find $\eta n = O(1)$. Next, we expand (54)

and (55) in the two small parameters, η and $\varphi = g - g_0$, and $n = n_0/\eta + n_1 + \cdots$ to obtain

$$t_1(\xi, g_0, n_0) + t_2(\xi, g_0, n_0, n_1)\varphi + \big(t_3(\xi, g_0, n_0, n_1)$$
$$+t_4(\xi, g_0, n_0, n_1, n_2)\varphi\big)\eta + \cdots = 0, \tag{61}$$
$$t_5(\xi, g_0, n_0) + t_4(\xi, g_0, n_0, n_1)\varphi + \big(t_6(\xi, g_0, n_0, n_1)$$
$$+t_7(\xi, g_0, n_0, n_1, n_2)\varphi\big)\eta + \cdots = 0. \tag{62}$$

For the leading-order balance, we find $\varphi = O(\eta)$. The leading orders of (61) and (62) are $t_1(\xi, g_0, n_0)$ and $t_2(\xi, g_0, n_0)$. The vanishing of these two terms yields the values of g_0 and n_0 that only depend on ξ. Next we seek an asymptotic solution for g_c and n_c in the following form

$$g_c = g_0 + g_1\eta + g_2\eta^2 + \cdots,$$
$$n_c = \eta^{-1}(n_0 + n_1\eta + n_2\eta^2 + \cdots), \tag{63}$$

where g_i and n_i $(i = 0, 1, 2, 3, \cdots)$ are function of ξ that can be deduced from (54) and (55). These expressions can only be solved semi-analytically and are listed in Appendix B.

Fig. 2 shows the normalized S1 solutions g_c/g_0 and $n_c\eta/n_0$ varying with η for fixed values of $\xi = 2, 4, 8, 16$, showing the influence of the curvature. The results in Fig. 2 demonstrate that both g_c/g_0 and $n_c\eta/n_0$ both increase linearly with η when ξ is small (≤ 8 in Fig. 2). For larger ξ values, when ξ increase from $O(1)$ to $O(\eta^{-1})$ (see e.g. $\xi = 16$ in Fig. 2), we see that the leading order of g_c/g_0 and $n_c\eta/n_0$ gradually turns from $1 + O(\eta)$ to $1 + O(\eta^2)$ [13, 19].

Stiff film on soft substrate S3: $\xi = O(\eta^{-3})$

For the flat case, k_c is $O(\xi^{-1/3}/h)$, and $n_c = O(\xi^{-1/3}/\eta)$. When $\xi = O(\eta^{-3})$, n_c is of order $O(1)$. In this situation, the assumption on large mode number needed to apply the WKB method is not satisfied. In this case, we need to solve (45-47). In order to obtain the general solution of (45), we use the fact that η is small to simplify α_f by taking the average value along the film thickness as

$$\alpha_f = \frac{1}{b-1}\int_1^b \alpha_f(r)dr = \frac{(B-1)g}{\sqrt{1 + (B^2-1)g^2} - 1}, \tag{64}$$

with $g = 1 + \epsilon$, where ϵ is a small parameter. Expanding α_f in ϵ yields:

$$\alpha_f = 1 - \frac{\epsilon}{B} + \frac{(2B^2 + B - 1)\epsilon^2}{2B^3} + O(\epsilon^3). \tag{65}$$

Substituting (65) into (45), the equation for U_f can now be solved as a regular perturbation problem:

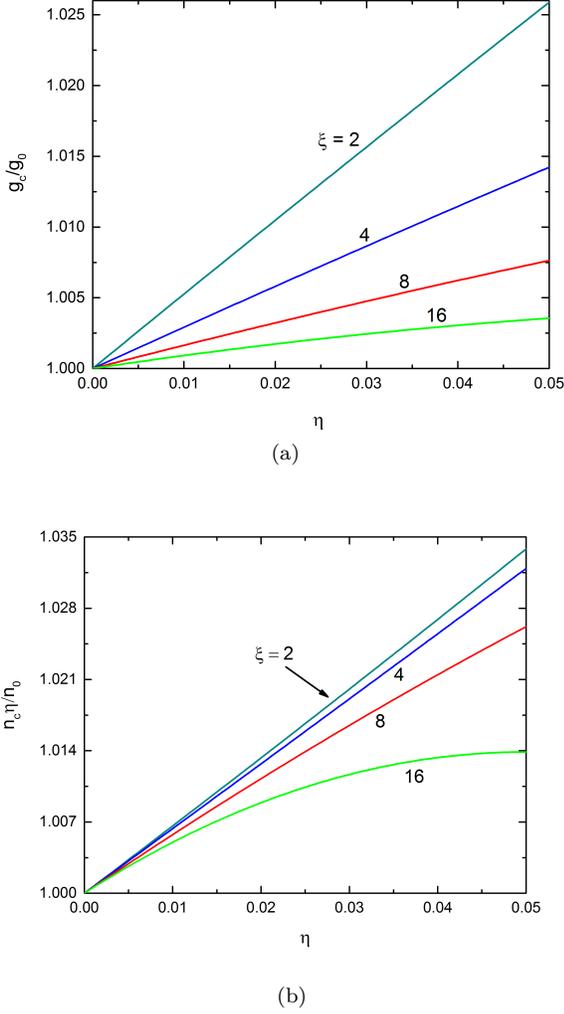$$U_f = U_{f0} + \epsilon U_{f1} + \epsilon^2 U_{f2} + \cdots, \tag{66}$$

(a)

(b)

FIG. 2. Normalized asymptotic results given by S1 for (a) g_c/g_0 and (b) $n_c\eta/n_0$ for various values of ξ.

and

$$U_{f0}^{(1)} = r^{-1-n}, \quad U_{f0}^{(2)} = r^{1-n},$$
$$U_{f0}^{(3)} = r^{1+n}, \quad U_{f0}^{(4)} = r^{-1+n},$$
$$U_{f1}^{(1)} = \frac{(n+2)r^{(-1-n)}(1 + 3n + n^2 + 2n(1+n)\ln(r))}{Bn(1+n)},$$
$$U_{f1}^{(2)} = 0, \quad U_{f1}^{(3)} = 0,$$
$$U_{f1}^{(4)} = -\frac{(n-2)r^{(-1+n)}(1 - 3n + n^2 + 2n(n-1)\ln(r))}{Bn(n-1)},$$
$$\cdots$$

Following the same steps as before, from a linear combination of these solutions we build a matrix $\mathbf{N}$ from the boundary conditions. The bifurcation condition is then given by $\mathbf{f}(\xi,\epsilon,\eta,n) \equiv \det(\mathbf{N}) = 0$, and $\mathbf{h}(\xi,\epsilon,\eta,n) \equiv \frac{\partial \mathbf{f}}{\partial n} = 0$. Expanding these two equations as series of ϵ

and η yields

$$t_0 + t_1\eta + t_2\eta\xi + t_3\eta^4\xi^2 + \left[t_4 + t_5\eta + (t_6\eta + t_7\eta^2)\xi \right.$$
$$\left. + (t_8\eta^2 + t_9\eta^3)\xi^2\right]\epsilon + \left[t_{10} + t_{11}\eta + (t_{12}\eta + t_{13}\eta^2)\xi \right.$$
$$\left. + (t_{14}\eta^2 + t_{15}\eta^3)\xi^2\right]\epsilon^2 + \cdots = 0, \tag{67}$$
$$q_0 + q_1\eta + q_2\eta\xi + q_3\eta^4\xi^2 + \left[q_4 + q_5\eta + (q_6\eta + q_7\eta^2)\xi \right.$$
$$\left. + (q_8\eta^2 + q_9\eta^3)\xi^2\right]\epsilon + \left[q_{10} + q_{11}\eta + (q_{12}\eta + q_{13}\eta^2\xi \right.$$
$$\left. + (q_{14}\eta^2 + q_{15}\eta^3)\xi^2\right]\epsilon^2 + \cdots = 0, \tag{68}$$

where t_i, q_i $(i = 1, 2, 3, \cdots)$ are polynomial functions of n. Since, $n = O(1)$, t_i and q_i are also of order $O(1)$. The leading-order terms of (67) are t_0, $t_2\eta\xi$, $t_3\eta^4\xi^2$, $t_8\eta^2\xi^2\epsilon$. We balance the latter three terms to obtain that $\eta\xi\epsilon = O(1)$. With the assumption $\xi = O(\eta^{-3})$ in this section, the order relation $\epsilon = O(\eta^2)$ can be deduced. Then, ξ can be written as $l_0\eta^{-3}$, and the asymptotic solution for g_c and n_c are as follows

$$g_c = 1 + g_1\eta^2 + g_2\eta^3 + g_3\eta^4 + \cdots$$
$$n_c = n_1 + n_2\eta + n_3\eta^2 + n_4\eta^3 + \cdots \tag{69}$$

where l_0 is a constant, and both g_i and n_i $(i = 1, 2, \cdots)$ are to be determined. Substituting equation (69) into (67, 68), the coefficients g_1 and n_1 can be deduced from the coefficients of the leading-order η^{-2} term. The first non-trivial mode is $n_c = 2$. With $n_c = 2$, only Equation (67) is needed and we have

$$g_c = 1 + \frac{1}{4\xi\eta} + \frac{3}{8\xi} + \frac{1 + 372\xi\eta^3}{48\xi^2\eta^2} + O(\eta^5). \tag{70}$$

Very stiff film on soft substrate S4: $\xi \gg O(\eta^{-3})$

Finally, we only keep the coefficient of ξ^2 in (67). From the leading-order terms, we deduce that $\epsilon = \eta^2$, and g_c is

$$g_c = 1 + g_1\eta^2 + g_2\eta^3 + g_3\eta^4 + \cdots, \tag{71}$$

where g_i $(i = 1, 2, 3, \cdots)$ are constants to be determined. Substituting (71) into the bifurcation condition (67) with $n_c = 2$, g_c can be obtained as

$$g_c = 1 + \frac{1}{4}\eta^2 + \frac{11}{96}\eta^4 + O(\eta^5). \tag{72}$$

Summary

In summary, we have four asymptotic solutions depending on the value of ξ:
(S1) When $\xi = O(1)$,

$$g_c = g_0 + g_1\eta + g_2\eta^2 + \cdots,$$
$$n_c = \eta^{-1}(n_0 + n_1\eta + n_2\eta^2 + \cdots). \tag{73}$$

(S2) When $\xi = O(\eta^{-1})$,

$$g_c = 1 + \frac{3^{2/3}}{4\xi^{2/3}} + \frac{17 \times 3^{1/3}}{160\xi^{4/3}} - \frac{3^{1/3}\xi^{2/3}}{12}\eta^2$$
$$- \frac{3^{2/3}}{4\xi^{2/3}}\eta + O(\eta^2), \tag{74}$$
$$n_c = \frac{3^{1/3}}{\xi^{1/3}\eta} - \frac{\xi}{3}\eta - \frac{11}{10\xi\eta} + \frac{3^{1/3}}{2\xi^{1/3}} + O(\eta^{2/3}).$$

(S3) When $\xi = O(\eta^{-3})$, we have $n_c = 2$, and

$$g_c = 1 + \frac{1}{4\xi\eta} + \frac{3}{8\xi} + \frac{1 + 372\xi\eta^3}{48\xi^2\eta^2} + O(\eta^5). \tag{75}$$

(S4) When $\xi \gg O(\eta^{-3})$, we have $n_c = 2$, and

$$g_c = 1 + \frac{1}{4}\eta^2 + \frac{11}{96}\eta^4 + O(\eta^5). \tag{76}$$

The first two solutions are obtained by assuming that n_c is large, so that the WKB method can be applied. In contrast, the last two solutions are obtained under the assumption that $n_c = O(1)$, and a regular perturbation method is used.

RESULTS AND DISCUSSION

In order to validate the theoretical solutions obtained in section , we compare the asymptotic solutions with numerical solutions based on calculating the Evans function via the compound matrix method, which can be easily extended to the case of two connected domains [28, 29], a Mathematica package implementation is available at github.com/SPPearce/CompoundMatrixMethod . Here we choose four values of $\eta = 0.1, 0.05, 0.01, 0.001$ for our simulations. Fig. 3 shows that the numerical results of g_c and $n_c\eta$ vary with $1/\xi$. In general, g_c and $n_c\eta$ increase with η and $1/\xi$. However, since n_c must be an integer, the graph of $n_c\eta$ is discontinuous as shown in Fig. 3b. The dashed lines in Fig. 3 represent the solution of the flat case from the work of Goriely and Alawiye [30]. With decreasing η, the cylindrical solutions are closer to the flat case. The solid line of $\eta = 0.001$ is almost undistinguishable with the dashed line, indicating that the cylinder can be treated as a flat solid when $\eta \leq 0.001$.

Comparisons between the asymptotic results and the numerical results for g_c and $n_c\eta$ are shown in Figs. 4 and 5, respectively. Taking the results of g_c when $\eta = 0.05$ as an example shown in Fig. 4a, the solid line denotes the numerical results and the dashed line with four parts denotes the asymptotic results in the four regimes denoted by S1, S2, S3, and S4. In Fig. 4a we see that the asymptotic results provide an excellent approximation to the numerical results in their respective regimes. However, in the regime where $\xi \in (O(\eta^{-3}), O(\eta^{-1}))$, neither asymptotic results of S2 and S3 match the numerical curve.

The main reason is that n_c is neither large enough so that the WKB method can be applied, nor close enough to $O(1)$ for a regular perturbation method. However, looking at $S1$ and $S2$ we see that the solution $S1$ is not only a nearly perfect fit to the numerical results in the region $\xi = O(1)$, it also covers the region of $S2$, where it provides a better agreement. Similar conclusions can be obtained in the case $\eta = 0.01$ in Fig. 4b. It is worth mentioning that the gap between region of S2 and S3 is reduced with decreasing η.

The comparison of results for $n_c\eta$ between asymptotic and numerical methods are shown in Fig. 5. Since $n_c = 2$ when $\xi \geq O(\eta^{-3})$, the four cases can be reduced to three cases with S4 merged into S3. Despite the fact that the asymptotic results are continuous for n_c, they provide good agreements as can be observed in Fig. 5. The S1 solution matches well with the numerical solution in a larger region even covering S2.

Together, from Figs. 4 and 5, we conclude that the asymptotic solutions match well with the numerical solutions, except for a gap between the domains of validity of S2 and S3. The solution of S2 can be substituted by S1. However, S2 has the advantage of being fully analytical, and can be used more conveniently if only focusing in region $\xi = O(\eta^{-1})$.

Next, we extend the region of $1/\xi$ to values larger than 1. Because of the large value of n_c in this region particularly for smaller values of η, this is numerically challenging, but we are able to solve this with the aid of the compound matrix method. Fig. 6 shows the S1 estimates for g_c and $n_c\eta$ when $\eta = 0.05, 0, 01$, and 0.001, compared to the flat solution [30]. For small η ($\eta = 0.001$), S1 is a very good fit for both g_c and $n_c\eta$ that is very close to the flat case. The critical growth parameter g_c increases with $1/\xi$ and η as shown in Fig. 6a. Fig. 6b shows that $n_c\eta$ increases with $1/\xi$ for a given value of η. The two solid curves with different η meet around $1/\xi = 1.14$, when the coefficient n_1 changes sign. Hence, $n_c\eta$ increase with η before this inflection point and decreases afterwards.

For the flat case, critical solutions exist for $1/\xi < 1/\xi_{min} \approx 1.895$ after which, the Biot instability [31] is the dominant wrinkling instability. This generic instability occurs when an elastic half plane subject to uniaxial compression becomes unstable with respect to zero wavelength wrinkles [30].
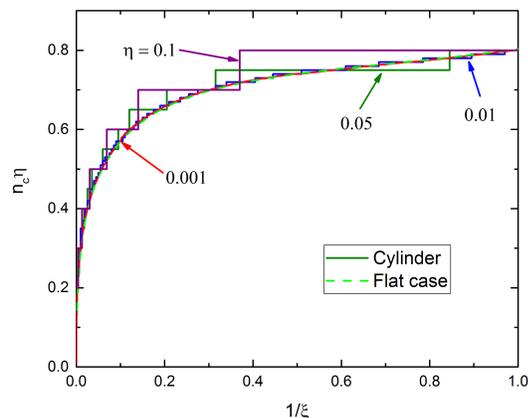
For the curved surfaces considered here, for large n, the eigenvalues tend towards a fixed asymptote that is independent of ξ, given by $g_{inf} = 2.6043, 2.1159, 1.8869, 1.8523$ respectively for $\eta = 0.1, 0.05, 0.01, 0.001$, corresponding to the Biot instability becoming dominant. As shown in Figure 6b, for $\eta = 0.01, 0.001$, the critical value of $n_c\eta$ approaches this value smoothly as $1/\xi$ is increased.
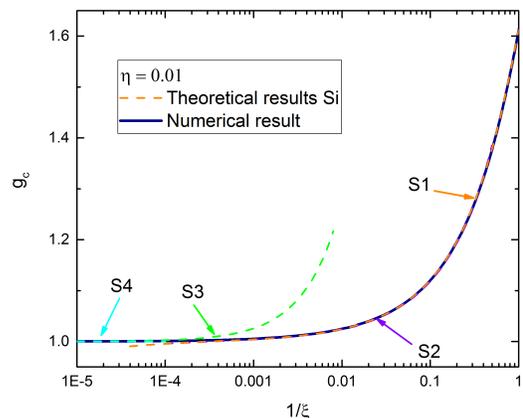
(a)
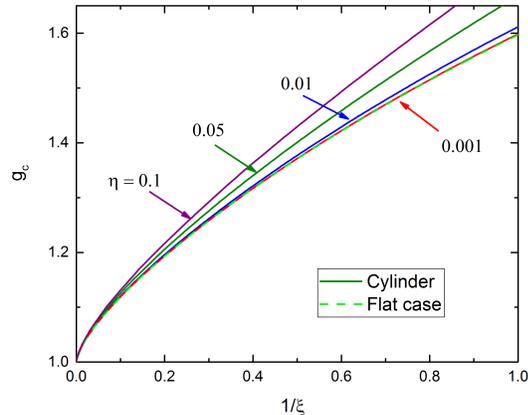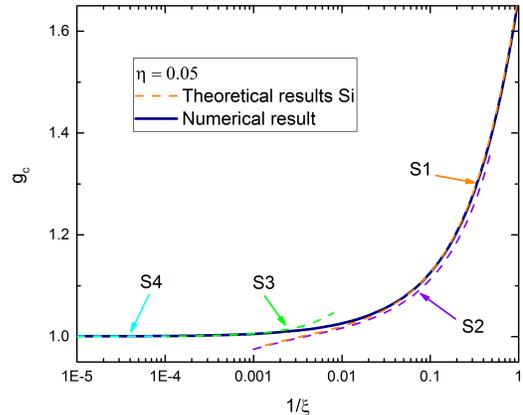
(b)

FIG. 3. Numerical solutions: (a)g_c and $n_c\eta$ (b) for various values of η.

(a)

(b)

FIG. 4. Comparison between asymptotic and numerical solution of g_c for $\eta = 0.05$ (a) and $\eta = 0.01$ (b). The solid line denotes the numerical results. The dashed lined is divided into four parts, S1, S2, S3, S4, representing the four sasymptotic regimes.

CONCLUSION

We studied the circumferential wrinkling of a growing cylinder tissues composed of a thin film on a cylindrical substrate. To bridge the gap between the classical planar case and the cylindrical case, we considered a cylinder with small ratio between the film thickness and the cylinder radius, that is $\eta \ll O(1)$. Under this assumption, we studied four regimes on the basis of the order relation between ξ and η. For each regime, we obtained asymptotic solutions for the critical growth g_c and wrinkling mode number n_c. Comparing these asymptotic solutions with numerical solutions, we showed that the asymptotic solutions provide a very good approximation in the corresponding regime. From this, we conclude that there is a systematic effect due to curvature: curvature delays the wrinkling instability. This implies that on a curved

surface with non-constant curvature, we expect to see a wrinkling pattern first forming first on those regions with the lowest curvature. Finally, while there is also a perturbation on the mode number due to the curvature, this effect is rather small and the mode number predicted by the theory of wrinkling on a flat substrate provides a good approximation for the problem.

The delay due to curvature is observed in simple models of brain morphogenesis consisting in the growth of a thin cortex over a growing ellipsoidal tissue representing white matter. In recent simulations of this growth process the wrinkle pattern first appear on regions with lower curvature [8, 32]. This effect is believed to be important in shaping the final gyral brain pattern based on the initial shape of the brain as originally proposed
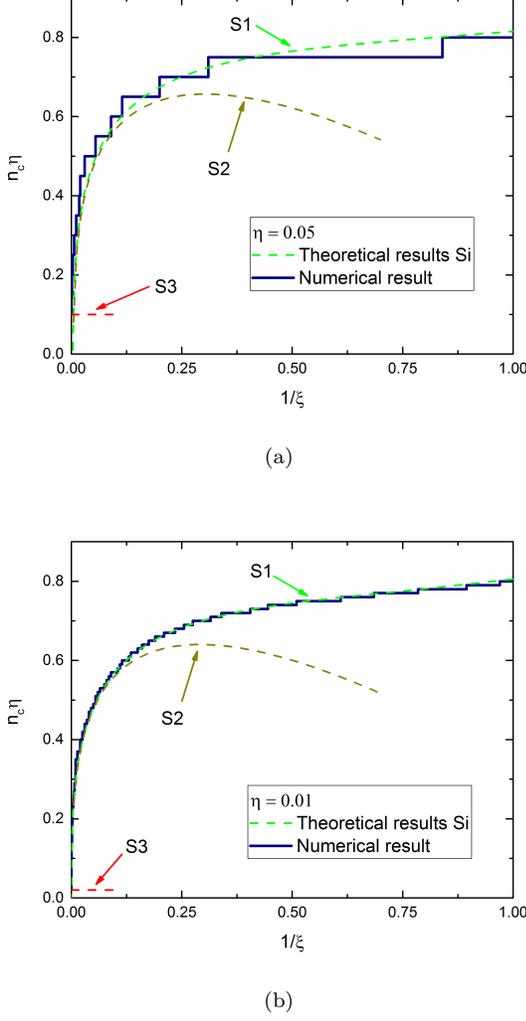
(a)

(b)

FIG. 5. Comparison between asymptotic and numerical solutions for $n\eta$ with $\eta = 0.05$ (a) and $\eta = 0.01$ (b). The solid line denotes the numerical results. The dashed line is divided into three parts, S1, S2, S3 (S4), representing the three regimes for $1/\xi$.

by Todd [33]. It is likely that the same interaction between geometry and pattern formation occurs in other problems of morphogenesis.

(a)

(b)
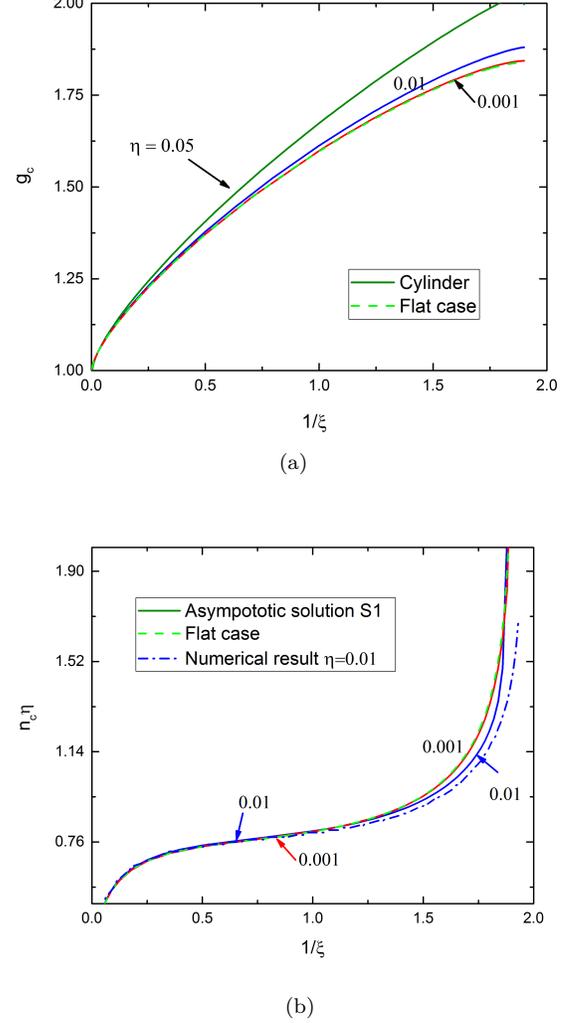
FIG. 6. The solution S1 for different values of η.

APPENDIX A

The matrix $\mathbf{M}$ can be expressed as

$$\mathbf{M} = \begin{bmatrix} G_{\mathrm{f}1}(b) & G_{\mathrm{f}2}(b) & G_{\mathrm{f}3}(b) & G_{\mathrm{f}4}(b) & 0 & 0 \\ H_{\mathrm{f}1}(b) & H_{\mathrm{f}2}(b) & H_{\mathrm{f}3}(b) & H_{\mathrm{f}4}(b) & 0 & 0 \\ E_1 G_{\mathrm{f}1}(a) & E_2 G_{\mathrm{f}2}(a) & E_3 G_{\mathrm{f}3}(a) & E_4 G_{\mathrm{f}4}(a) & G_{\mathrm{s}1}(a) & G_{\mathrm{s}2}(a) \\ E_1 H_{\mathrm{f}1}(a) & E_2 H_{\mathrm{f}2}(a) & E_3 H_{\mathrm{f}3}(a) & E_4 H_{\mathrm{f}4}(a) & H_{\mathrm{s}1}(a) & H_{\mathrm{s}2}(a) \\ E_1 & E_2 & E_3 & E_4 & -U_{\mathrm{s}}^{(1)}(a) & -U_{\mathrm{s}}^{(2)}(a) \\ -E_1 S_{\mathrm{f}}^{(1)}(a) & -E_2 S_{\mathrm{f}}^{(2)}(a) & -E_3 S_{\mathrm{f}}^{(3)}(a) & -E_4 S_{\mathrm{f}}^{(4)}(a) & -U_{\mathrm{s}}^{'(1)}(a) & -U_{\mathrm{s}}^{'(2)}(a) \end{bmatrix}, \tag{A.1}$$

TABLE I. g_i and n_i varying with ξ

ξ	g_0	n_0	g_1	n_1	g_2	n_2
2.	1.37062	0.740338	0.723767	0.486206	-0.287175	0.292942
4.	1.22646	0.679204	0.360783	0.430743	-0.237694	0.0525033
6.	1.16985	0.633439	0.246533	0.384075	-0.27418	-0.330524
8.	1.13867	0.597837	0.190279	0.351907	-0.329063	-0.776405
10.	1.11858	0.569193	0.15658	0.328198	-0.38857	-1.25895
12.	1.1044	0.545474	0.134014	0.309761	-0.448778	-1.76607
14.	1.09379	0.525376	0.117774	0.294856	-0.508344	-2.291
16.	1.08549	0.508032	0.105483	0.282454	-0.566788	-2.82954
18.	1.0788	0.49284	0.0958289	0.271905	-0.623954	-3.37889
20.	1.07327	0.47937	0.0880259	0.262773	-0.679825	-3.93704
22.	1.06861	0.467305	0.0815751	0.254758	-0.734439	-4.50253
24.	1.06462	0.456405	0.0761434	0.247639	-0.787859	-5.07425
26.	1.06117	0.446485	0.0715	0.241256	-0.840152	-5.65134
28.	1.05813	0.437399	0.0674796	0.235484	-0.89139	-6.2331
30.	1.05545	0.429031	0.0639606	0.230229	-0.941638	-6.81898
32.	1.05305	0.421286	0.0608515	0.225414	-0.99096	-7.40852
34.	1.0509	0.414086	0.0580822	0.220979	-1.03941	-8.00133
36.	1.04895	0.407368	0.0555977	0.216874	-1.08705	-8.59709
38.	1.04717	0.401076	0.0533546	0.213059	-1.13391	-9.19553
40.	1.04555	0.395166	0.0513181	0.209499	-1.18005	-9.79641

FIG. 7. g_i $(i = 0, 1, 2)$ varying with ξ.

with

$$E_i = \exp\left(\int_1^b S_{\mathrm{f}}^{(i)}(r)\mathrm{d}r\right),$$

$$\begin{aligned}G_{\mathrm{f}i}(r) = \frac{\xi}{\alpha_{\mathrm{f}}^2 r^3}\Big[&1 - n^2 - r^3 S_{\mathrm{f}}^{(i)3} + 2r^2 S_{\mathrm{f}}^{(i)2}(1 + \alpha_{\mathrm{f}}^2)\\ &- 2r^2 S_{\mathrm{f}}^{(i)'} + 2\alpha_{\mathrm{f}}^2(-1 + n^2 - r^2 S_{\mathrm{f}}^{(i)'}) - r^3 S_{\mathrm{f}}^{(i)''}\\ &+ r S_{\mathrm{f}}^{(i)}(1 + 2n^2 - 2\alpha_{\mathrm{f}}^2 + n^2\alpha_{\mathrm{f}}^4 + 3r^2 S_{\mathrm{f}}^{(i)'})\Big],\end{aligned}$$

$$H_{\mathrm{f}i}(r) = \frac{\xi}{\alpha_{\mathrm{f}}^2 r^2}(n^2 - 1 - r S_{\mathrm{f}}^{(i)} + r^2 S_{\mathrm{f}}^{(i)2} - r^2 S_{\mathrm{f}}^{(i)'}),$$

$$G_{\mathrm{s}1}(r) = 2n(n^2 - n - 2)r^{n-2},$$

$$G_{\mathrm{s}2}(r) = 2(n-1)n^2 r^{n-4},$$

$$H_{\mathrm{s}1}(r) = -2n(1+n)r^{n-1},$$

$$H_{\mathrm{s}2}(r) = -2n(n-1)r^{n-3}.$$

APPENDIX B

Here we give some semi-analytical results for the case S1 under the given value of ξ (see table I). Fig. 7 shows g_0, g_1 and g_2 varying with ξ. In the region $\xi \in [2, 40]$, g_1 decreases dramatically with ξ represents that the curvature has less effects on g_{c} with large ξ. Since g_1 and n_1 are positive, it means that the curvature increases g_{c} and k_{c} in this region.
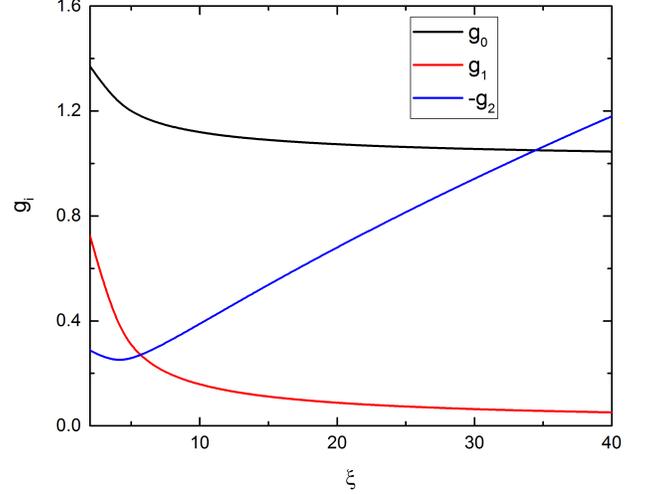
[1] Bo Li, Yan-Ping Cao, Xi-Qiao Feng, and Huajian Gao. Mechanics of morphological instabilities and surface wrinkling in soft materials: a review. Soft Matter, 8 (21):5728–5745, 2012.

[2] Silvia Budday, Sebastian Andres, Bastian Walter, Paul Steinmann, and Ellen Kuhl. Wrinkling instabilities in soft bilayered systems. Phil. Trans. R. Soc. A, 375(2093): 20160163, 2017.

[3] Alain Goriely. The mathematics and mechanics of biological growth, volume 45. Springer, 2017.

[4] Martine Ben Amar and Fei Jia. Anisotropic growth shapes intestinal tissues during embryogenesis. Proceedings of the National Academy of Sciences, 110 (26):10525–10530, 2013.

[5] Silvia Budday, Ellen Kuhl, and John W Hutchinson. Period-doubling and period-tripling in growing bilayered systems. Philosophical Magazine, 95(28-30):3208–3224, 2015.

[6] P Nardinocchi and E Puntel. Swelling-induced wrinkling in layered gel beams. Proc. R. Soc. A, 473(2207): 20170454, 2017.

[7] Lihua Jin, Dayong Chen, Ryan C Hayward, and Zhigang Suo. Creases on the interface between two soft materials. Soft Matter, 10(2):303–311, 2014.

[8] Silvia Budday, Paul Steinmann, Alain Goriely, and Ellen Kuhl. Size and curvature regulate pattern selection in the mammalian brain. Extreme Mechanics Letters, 4: 193–198, 2015.

[9] Martine Ben Amar and Adrien Bordner. Mimicking cortex convolutions through the wrinkling of growing soft bilayers. Journal of Elasticity, 129(1-2):213–238, 2017.

[10] Cheng Zhang, Bo Li, Xiao Huang, Yong Ni, and Xi-Qiao Feng. Morphomechanics of bacterial biofilms undergoing anisotropic differential growth. Applied Physics Letters, 109(14):143701, 2016.

[11] Pasquale Ciarletta and Martine Ben Amar. Papillary networks in the dermal–epidermal junction of skin: a biomechanical model. Mechanics Research Communications, 42:68–76, 2012.

[12] Fei Jia and Martine Ben Amar. Theoretical analysis of growth or swelling wrinkles on constrained soft slabs. Soft Matter, 9(34):8216–8226, 2013.

[13] Shengqiang Cai, Derek Breid, Alfred J Crosby, Zhigang Suo, and John W Hutchinson. Periodic patterns and energy states of buckled films on compliant substrates. Journal of the Mechanics and Physics of Solids, 59(5): 1094–1114, 2011.

[14] Yan Zhao, Xue Han, Guoyang Li, Conghua Lu, Yanping Cao, Xi-Qiao Feng, and Huajian Gao. Effect of lateral dimension on the surface wrinkling of a thin film on compliant substrate induced by differential growth/swelling. Journal of the Mechanics and Physics of Solids, 83:129–145, 2015.

[15] Bo Li, Yan-Ping Cao, Xi-Qiao Feng, and Huajian Gao. Surface wrinkling of mucosa induced by volumetric growth: theory, simulation and experiment. Journal of the Mechanics and Physics of Solids, 59(4):758–774, 2011.

[16] Fan Xu, Radhi Abdelmoula, and Michel Potier-Ferry. On the buckling and post-buckling of core-shell cylinders under thermal loading. International Journal of Solids and Structures, 126:17–36, 2017.

[17] Pedro Patrício, Paulo Ivo Cortez Teixeira, AC Trindade, and MH Godinho. Longitudinal versus polar wrinkling of core-shell fibers with anisotropic size mismatches. Physical Review E, 89(1):012403, 2014.

[18] Bo Li, Fei Jia, Yan-Ping Cao, Xi-Qiao Feng, and Huajian Gao. Surface wrinkling patterns on a core-shell soft sphere. Physical review letters, 106(23):234301, 2011.

[19] Norbert Stoop, Romain Lagrange, Denis Terwagne, Pedro M Reis, and Jörn Dunkel. Curvature-induced symmetry breaking determines elastic surface patterns. Nature materials, 14(3):337, 2015.

[20] Jie Yin, Zexian Cao, Chaorong Li, Izhak Sheinman, and Xi Chen. Stress-driven buckling patterns in spheroidal core/shell structures. Proceedings of the National Academy of Sciences, 105(49):19132–19135, 2008.

[21] AC Trindade, João P Canejo, LFV Pinto, Pedro Patrício, P Brogueira, Paulo Ivo Cortez Teixeira, and MH Godinho. Wrinkling labyrinth patterns on elastomeric janus particles. Macromolecules, 44(7):2220–2228, 2011.

[22] Fan Xu and Michel Potier-Ferry. Quantitative predictions of diverse wrinkling patterns in film/substrate systems. Scientific reports, 7(1):18081, 2017.

[23] Lishuai Jin, Yang Liu, and Zongxi Cai. Asymptotic solutions on the circumferential wrinkling of growing tubular tissues. International Journal of Engineering Science, 128:31–43, 2018.

[24] M Sanjarani Pour. WKB analysis of the buckling of a neo-Hookean cylindrical shell of arbitrary thickness subject to an external pressure. International Journal of Applied Mechanics, 2(04):857–870, 2010.

[25] Yibin Fu. Some asymptotic results concerning the buckling of a spherical shell of arbitrary thickness. International journal of non-linear mechanics, 33(6): 1111–1122, 1998.

[31] Maurice A Biot. Surface instability of rubber in compression. Applied Scientific Research, Section A, 12(2): 168–182, 1963.

[26] Martine Ben Amar and Alain Goriely. Growth and instability in elastic tissues. Journal of the Mechanics and Physics of Solids, 53(10):2284–2319, 2005.

[27] Fei Jia, Bo Li, Yan-Ping Cao, Wei-Hua Xie, and Xi-Qiao Feng. Wrinkling pattern evolution of cylindrical biological tissues with differential growth. Physical Review E, 91(1):012403, 2015.

[28] Nitin R Anturkar, Tasos C Papanastasiou, and James O Wilkes. Compound matrix method for eigenvalue problems in multiple connected domains. Communications in applied numerical methods, 8(11):811–818, 1992.

[29] Sara Roccabianca, Davide Bigoni, and Massimiliano Gei. Long wavelength bifurcations and multiple neutral axes of elastic layered structures subject to finite bending. Journal of Mechanics of Materials and Structures, 6(1): 511–527, 2011.

[30] Alain Goriely and Hamza Alawiye. The wrinkling problem revisited: A nonlinear analysis. Preprint, 2018.

[32] PV Bayly, RJ Okamoto, G Xu, Y Shi, and LA Taber. A cortical folding model incorporating stress-dependent growth explains gyral wavelengths and stress patterns in the developing brain. Physical biology, 10(1):016005, 2013.

[33] PH Todd. A geometric model for the cortical folding pattern of simple folded brains. Journal of theoretical biology, 97(3):529–538, 1982.